# Surface wave holography on designing subwavelength metallic structures

**Yu-Hui Chen, Jin-Xin Fu, and Zhi-Yuan Li***

*Laboratory of Optical Physics, National Laboratory for Condensed Matter Physics, Institute of Physics, Chinese Academy of Science, Beijing 100190, China*

*lizy@aphy.iphy.ac.cn*

**Abstract:** We report a method in the framework of surface wave holography to manipulate the electromagnetic wave on the metallic surface for realizing complicated electromagnetic wave transport functionalities in three-dimensional (3D) space. The method allows for direct determination of the metallic surface structure morphology for a given transport functionality, by means of writing desirable object information on the metallic surface via interference with a reference surface wave. We have employed the analytical approach to design and build metallic surface structures that realize arbitrary single-point focusing, arbitrary single-direction beam collimation, and simultaneous two-point focusing of electromagnetic wave in 3D space. Good agreement between numerical simulations and microwave experimental measurements has been found and confirms the power of the method in conceptually understanding and exploiting the surface electromagnetic wave on subwavelength metal structures.



**OCIS codes:** (090.2910) Holography, microwave; (240.6690) Surface waves; (310.6628) Subwavelength structures, nanostructures; (310.6845) Thin film devices and applications.

## References and links

1. C. Genet and T. W. Ebbesen, "Light in tiny holes," Nature **445**(7123), 39–46 (2007).
2. T. W. Ebbesen, H. J. Lezec, H. F. Ghaemi, T. Thio, and P. A. Wolff, "Extraordinary optical transmission through sub-wavelength hole arrays," Nature **391**(6668), 667–669 (1998).
3. H. J. Lezec, A. Degiron, E. Devaux, R. A. Linke, L. Martin-Moreno, F. J. Garcia-Vidal, and T. W. Ebbesen, "Beaming light from a subwavelength aperture," Science **297**(5582), 820–822 (2002).
4. G. A. Zheng, X. Q. Cui, and C. H. Yang, "Surface-wave-enabled darkfield aperture for background suppression during weak signal detection," Proc. Natl. Acad. Sci. U.S.A. **107**(20), 9043–9048 (2010).
5. W. Srituravanich, N. Fang, C. Sun, Q. Luo, and X. Zhang, "Plasmonic nanolithography," Nano Lett. **4**(6), 1085–1088 (2004).
6. B. Lee, S. Kim, H. Kim, and Y. Lim, "The use of plasmonics in light beaming and focusing," Prog. Quantum Electron. **34**(2), 47–87 (2010).
7. N. Yu, J. Fan, Q. J. Wang, C. Pflügl, L. Diehl, T. Edamura, M. Yamanishi, H. Kan, and F. Capasso, "Small-divergence semiconductor lasers by plasmonic collimation," Nat. Photonics **2**(9), 564–570 (2008).
8. A. P. Hibbins, J. R. Sambles, and C. R. Lawrence, "Gratingless enhanced microwave transmission through a subwavelength aperture in a thick metal plate," Appl. Phys. Lett. **81**(24), 4661–4663 (2002).
9. H. Caglayan, I. Bulu, and E. Ozbay, "Observation of off-axis directional beaming via subwavelength asymmetric metallic gratings," J. Phys. D Appl. Phys. **42**(4), 045105 (2009).
10. L. Martín-Moreno, F. J. García-Vidal, H. J. Lezec, A. Degiron, and T. W. Ebbesen, "Theory of highly directional emission from a single subwavelength aperture surrounded by surface corrugations," Phys. Rev. Lett. **90**(16), 167401 (2003).
11. J. J. Cowan, "The surface ace plasmon resonance effect in holography," Opt. Commun. **5**(2), 69–72 (1972).
12. J. J. Cowan, "Holography with Standing Surface Plasma-Waves," Opt. Commun. **12**(4), 373–378 (1974).
13. S. Maruo, O. Nakamura, and S. Kawata, "Evanescent-wave holography by use of surface-plasmon resonance," Appl. Opt. **36**(11), 2343–2346 (1997).
14. M. Ozaki, J. Kato, and S. Kawata, "Surface-plasmon holography with white-light illumination," Science **332**(6026), 218–220 (2011).
15. S. A. Maier, *Plasmonics: Fundamentals and Applications* (Springer, 2006).
16. H. J. Lezec and T. Thio, "Diffracted evanescent wave model for enhanced and suppressed optical transmission through subwavelength hole arrays," Opt. Express **12**(16), 3629–3651 (2004).

#149847 - $15.00 USD Received 24 Jun 2011; revised 2 Sep 2011; accepted 23 Oct 2011; published 10 Nov 2011

17. G. Gay, O. Alloschery, B. Viaris de Lesegno, C. O'Dwyer, J. Weiner, and H. J. Lezec, "The optical response of nanostructured surfaces and the composite diffracted evanescent wave model," Nat. Phys. **2**(4), 262–267 (2006).
18. P. Lalanne and J. P. Hugonin, "Interaction between optical nano-objects at metallo-dielectric interfaces," Nat. Phys. **2**(8), 551–556 (2006).
19. H. T. Liu and P. Lalanne, "Microscopic theory of the extraordinary optical transmission," Nature **452**(7188), 728–731 (2008).
20. J. B. Pendry, L. Martín-Moreno, and F. J. Garcia-Vidal, "Mimicking surface plasmons with structured surfaces," Science **305**(5685), 847–848 (2004).
21. F. J. Garcia-Vidal, L. Martin-Moreno, and J. B. Pendry, "Surfaces with holes in them: new plasmonic metamaterials," J. Opt. A, Pure Appl. Opt. **7**(2), 97–101 (2005).
22. J. Seidel, S. Grafstrom, L. Eng, and L. Bischoff, "Surface plasmon transmission across narrow grooves in thin silver films," Appl. Phys. Lett. **82**(9), 1368–1370 (2003).
23. R. A. Flynn, I. Vurgaftman, K. Bussmann, B. S. Simpkins, C. S. Kim, and J. P. Long, "Transmission efficiency of surface plasmon polaritons across gaps in gold waveguides," Appl. Phys. Lett. **96**(11), 111101 (2010).
24. J. W. Goodman, "Introduction to principles and applications of holography," Pr. Inst. Electr. Elect. **59**, 1292–1304 (1971).
25. H. A. Bethe, "Theory of diffraction by small holes," Phys. Rev. **66**(7-8), 163–182 (1944).
26. M. Huang, F. L. Zhao, Y. Cheng, N. S. Xu, and Z. Z. Xu, "Origin of laser-induced near-subwavelength ripples: interference between surface plasmons and incident laser," ACS Nano **3**(12), 4062–4070 (2009).
27. L. B. Yu, D. Z. Lin, Y. C. Chen, Y. C. Chang, K. T. Huang, J. W. Liaw, J. T. Yeh, J. M. Liu, C. S. Yeh, and C. K. Lee, "Physical origin of directional beaming emitted from a subwavelength slit," Phys. Rev. B **71**(4), 041405 (2005).

## 1. Introduction

Subwavelength structures on a metallic surface have attracted much interest over years [1]. Many extraordinary properties occur when modulating the metallic surface with subwavelength structures [1–3]. When a subwavelength aperture is surrounded by periodic corrugations, the transmitted light can emerges as a beam with a small angular divergence, instead of diffracting in all directions [3]. This finding has opened a path to get a high energy collection without losing the subwavelength resolution. Later on, many structures have been proposed to realize and utilize the focusing and collimation of light on a corrugated metallic surface [4–9]. It is believed that the interaction between surface electromagnetic wave and subwavelength metallic structures plays a key role in the focusing and beaming phenomenon [2, 6, 10].

So far, an analytical tool that allows for easy conceptual understanding of the numerical or experimental results of metallic surface periodic structures is absent, and this becomes a big obstacle for expanding these structures to have more complicated functionalities. In this work, by introducing the concept of surface wave holography [11–14], we find that the extensively studied focusing and beaming structures [3, 6], metallic films with a hole surrounding by grooves etc., are essentially a plane hologram [11–14]. We present an analytical approach in the framework of surface wave holography to manipulate the electromagnetic wave through a subwavelength hole on the metallic surface. For a given electromagnetic wave transportation, one can determine the surface morphology of a metallic plate easily by using the proposed method. Focusing and beaming are considered as examples and confirmed numerically and experimentally.

The paper is organized as follows. In Section 2, we investigate the scattering behavior of surface electromagnetic wave by small grooves in a metal plate, whose size is much smaller than wavelength. It shows that almost all energy would pass through the grooves and the phase shift can be ignored. Based on these properties, an analytical theory using surface wave to realize holography is proposed in Section 3, with both the recording and reconstituting processes demonstrated. In Sections 4 and 5, we treat an arbitrarily focusing in 3D space as a special case of holography, *viz.*, a single-point imaging, and a beaming effect in any solid angle as an image of a plane wave. Both numerical and experimental results are shown. A two-point imaging is further presented in Section 6, which shows the feasibility of writing independent objects on the same metal plate. Finally in Section 7 we summarize this paper. All simulations in this paper are carried out with finite-difference time-domain (FDTD) method for microwave or visible regime, while our experiments are performed in the microwave frequencies.

#149847 - $15.00 USD Received 24 Jun 2011; revised 2 Sep 2011; accepted 23 Oct 2011; published 10 Nov 2011

## 2. Small groove scattering

We start from a two-dimensional (2D) metallic structure whose geometry is shown in Fig. 1(a). When electromagnetic wave passes a subwavelength aperture, surface wave can be excited. The components of the surface wave are complicated, including the surface plasmon polariton (SPP), which is a localized surface mode [15], and a diffracted evanescent wave (DEW) [16–19]. What's more, a perfectly conducting surface with periodic corrugations also supports surface bound modes [20, 21]. The excited surface wave is then scattered by a small groove located at a distance from the center. In our microwave simulation, the wavelength of the electromagnetic considered is 20 mm and the thickness of the metal plate is 3 mm. The subwavelength aperture has a radius equal to 4 mm and is located at $x = 0$ mm. The center of a 2 mm wide and 1.5 mm deep groove is located at $x = 18$ mm. At 10 mm beneath the aperture, a source is situated with its polarization parallel to the $x$ axis, as illustrated in Fig. 1(a). The information of electromagnetic wave immediately above the metal surface is collected to study the transport behavior of the surface wave.

From Fig. 1(b) we can tell that most energy of the surface wave passes through when it meets a groove. At the edge of the aperture and the groove, sharp peaks appear, which is due to the local field enhancement of metal. Figure 1(c) shows that the phases of $E_x$ and $E_y$ vary along the $x$ axis, with and without a groove, while the phases at the edge of the aperture, *viz.*, $x = 4$mm, are set to be 0. For clarity the curve of $E_y$ (upper one) is vertically offset. We can see that in the vicinity of the groove, the phases of both $E_x$ and $E_y$ differ from those without a groove, but beyond a very short distance from the groove the additional phase shifts can be ignored.

#149847 - $15.00 USD Received 24 Jun 2011; revised 2 Sep 2011; accepted 23 Oct 2011; published 10 Nov 2011

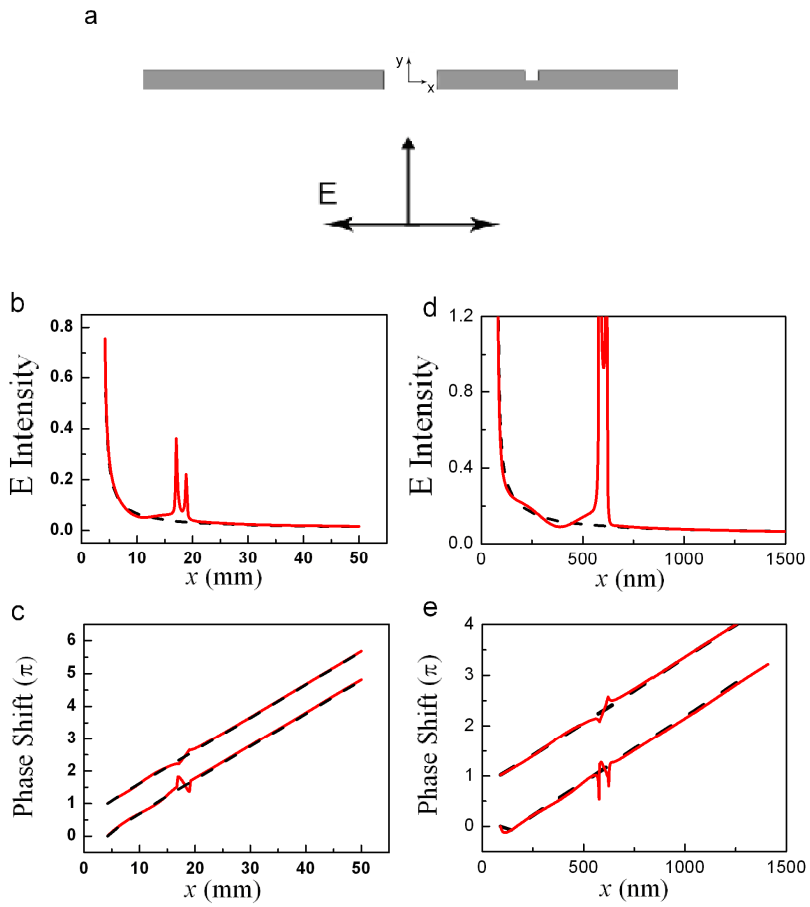


Fig. 1. Simulation of groove scattering for a metallic subwavelength structure depicted in panel (a). Field intensity and phase profile for microwave [panels (b) and (c)], and 633 nm visible light [panels (d) and (e)]. (b) Normalized intensity immediately above the metal film with (red solid) and without (black dash) a groove located at $x$ = 18 mm, from the edge of the aperture $x$ = 4 mm to $x$ = 50 mm. (c) Phase varying with distance relative to the edge of the aperture (the phase at $x$ = 4 mm is set to be 0.) with (red solid) and without (black dash) a groove at $x$ = 18 mm. Phase of components $E_x$ and $E_y$ are shown. For clarity, $E_y$ (upper one) is vertically offset. (d) Normalized intensity immediately above the metal film with (red solid) and without (black dash) a groove located at $x$ = 600 nm. (c) Phase varying with distance relative to the edge of the aperture (the phase at $x$ = 90 nm is set to be 0.) with (red solid) and without (black dash) a groove at $x$ = 600 nm. Phase of components $E_x$ and $E_y$ are shown. For clarity, $E_y$ (upper one) is vertically offset.

Simulations for visible light are also performed using a similar structure in Ag film and 633 nm light. Parameters of the structure are: the film thickness 150 nm, the location of hole (0,0), the width of the hole 150 nm, the location of the groove 600 nm, and the width and depth of the groove both 40 nm. The results indicate that they share the same characteristics as the microwave structure, as shown in Fig. 1(d) and 1(e). Previous experimental studies [22, 23] showed that the transmittance of SPP is very high when it passes through a gap, which is consistent with our calculation here.

The above analysis indicates that when surface wave passes a groove, the change of both intensity and phase is negligible due to the small scale of the groove. This characteristic is important for the surface wave holography, as will be shown below. What is more, the simulation results in Fig. 1 show that the field intensity has a maximum right at the groove, which is much larger than at other positions outside the groove. This means the field

#149847 - $15.00 USD Received 24 Jun 2011; revised 2 Sep 2011; accepted 23 Oct 2011; published 10 Nov 2011

distribution immediately above the metal film can be well modeled and approximated by a δ function (the scale of groove is much smaller than wavelength). Such an assumption is used in Section 3.

### 3. Theory of surface electromagnetic wave holography

A brief look back to the conventional optical holography might be helpful to illustrate our ideas. It is well known that two essential steps are involved in the conventional holography, *viz.*, first the recording and later the reconstruction of the amplitude and phase distribution of an incident wave [11, 13, 24]. In the process of recording, two laser light waves shine on the recording thin film, e.g., an emulsion. One is the reflected or transmitted wave that comes from the object that we are interested in, and is therefore named the "object" wave denoted by $U_0(x, y)$. The other wave is the "reference" wave, which is used to interfere with the object wave and write the interference fringes on the emulsion, and we denote it by $U_w(x, y)$. In the process of image reconstitution, in order to read the structures on the exposed emulsion, another reference wave $U_r(x, y)$ is needed, which is identical to $U_w(x, y)$ in most cases.

In this paper the structure we focus on is a subwavelength hole surrounded by grooves, thus we first restrict the source of surface wave to a subwavelength hole on a metal plate, as shown in Fig. 2(a). A perforated metal film is situated at $z = 0$ plane, with an aperture located at (0, 0, 0). Surface wave is excited by shining the aperture from $z<0$ region. The radius of the aperture is much smaller than the wavelength so that the transmission is weak [25] and the directly transmitted wave would not affect the scattering field significantly.

Similar to the conventional optical holography, the surface electromagnetic wave holography involves writing and reading processes [11, 13]. In the writing process, the writing reference wave is the surface wave excited by the subwavelength hole, $U_w = A_w(x, y)\exp[i(\varphi_w + n_{eff}kr)]$, where $\varphi_w$ is the initial phase, $n_{eff}$ the index of the surface wave, $k$ the norm of vacuum wave vector, and $A_w(x, y)$ the amplitude. The object wave carrying the object information shines on the metal film with the complex amplitude at the metal plate $U_0 = A_0(x, y)\exp[i\psi_0(x, y)]$. Then the interference fringes of $U_0$ and $U_w$ will appear [26], and we need to store the information of the interference ripples and then read it out. The intensity distribution of the interference pattern on the metal film is:

$$\begin{aligned} I(x, y) &= [U_0(x, y) + U_w(x, y)] \times [U_0^*(x, y) + U_w^*(x, y)] \\ &= U_0U_0^* + U_wU_w^* + U_0U_w^* + U_0^*U_w \\ &= A_0^2 + A_w^2 + U_0U_w^* + U_0^*U_w \end{aligned} \tag{1}$$

The maxima occur at

$$\psi_0 - \varphi_w - n_{eff}kr - 2m\pi = 0 \tag{2}$$

where m = 0, ± 1, ± 2…Different from the conventional optical holography, we carve small grooves on our sample only around the maxima of $I(x, y)$, leaving the rest flat, as shown in Fig. 2(b). Due to the grooves, field intensity maxima appear at the position of grooves when surface wave propagates on such milled surface, as shown in Fig. 1. Considering that the scale of grooves is much smaller than the wavelength, typically $\lambda/10$, we can introduce the discrete approximation by using a $\delta$ function to express the grooves' effect on surface wave. Then the surface wave scattering function of the modulated metal plate is

$$G(x, y) = \sum_m G_m(x, y) = \sum_m \alpha_m(x, y)\delta(\psi_0 - \varphi_w - n_{eff}kr - 2m\pi) \tag{3}$$

$G(x, y)$ stands for the scattering strength at any given point $(x, y)$, which means that only at the positions of grooves, $\psi_0 - \varphi_w - n_{eff}kr - 2m\pi = 0$, does the scattering of surface wave arise. Here we take the groove width as infinite narrow, however, in reality it is impossible and the widths [22, 23] and depths of grooves can have influence on the intensity of the scattered

#149847 - $15.00 USD Received 24 Jun 2011; revised 2 Sep 2011; accepted 23 Oct 2011; published 10 Nov 2011

wave. Thus we introduce $\alpha_m(x,y)$, a scattering coefficient, to describe the scattered wave intensity due to the details of the grooves, such as the widths and depths. $G(x, y)$ here can be looked upon as the transfer function of the surface wave structure, which is similar to the transfer function of a lens.

To accomplish the reading process, we need another surface wave to read the structures recorded on the metal plate and reconstitute the image. As the perturbation of the narrow grooves on the surface wave is negligible, we can write down the reading surface wave as $U_r = A_r(x, y)\exp[i(\varphi_r + n_{eff}kr)]$, the same form as $U_w$, although many grooves are carved on the metal plate. This feature provides a lot of conveniences in designing the scattered wave front. The reading wave interacts with the grooves, and the strength of the scattered wave immediately above the metal plate is

$$\begin{aligned} S(x, y) &= U_r(x, y)G(x, y) \\ &= \sum_m \alpha_m \delta(\psi_0 - \varphi_w - n_{eff}kr - 2m\pi)A_r \exp[i(\varphi_r + n_{eff}kr)] \end{aligned} \tag{4}$$

$S(x, y)$ propagates in the upper space and then reconstitutes the image that we need. According to Huygens–Fresnel principle, the complex amplitude at any point $(p, q, l)$ in the upper space is a sum added up by the scattered waves from all the point sources:

$$U_{img}(p,q,l) \propto \int_G S(x,y)\frac{\exp[ik\sqrt{(p-x)^2+(q-y)^2+l^2}]}{\sqrt{(p-x)^2+(q-y)^2+l^2}}dxdy \tag{5}$$

The integral is carried out on the "exposed" metal plane. Inserting Eq. (4) into Eq. (5) and using the integral characteristics of $\delta$ function, we obtain

$$U_{img}(p,q,l) \propto \sum_m \int_{G_m} \alpha_m A_r \frac{\exp\{i[k\sqrt{(p-x)^2+(q-y)^2+l^2}+\psi_o - 2m\pi]\}}{\sqrt{(p-x)^2+(q-y)^2+l^2}}ds \tag{6}$$

Here $\varphi_w = \varphi_r = 0$ is chosen. The integral is a curve integral which is carried out along the curve $G_m$[curves in Eq. (3)].

It is worth reemphasizing several assumptions that we use to deduce Eq. (6). Firstly, given the electromagnetic field distribution of a surface, one can deduce the field at any point out of source by using Huygens–Fresnel principle as only electromagnetic waves propagating in free space is involved. The exact field distribution on the metal surface is much too complicated and we just approximately use a $\delta$ function to model it. Secondly, we treat each polarization component of the electromagnetic field independently, for the reason that all of them satisfy Helmholtz equation in the free space. Equations (3)–(6) can be regarded as equations for any single polarization component. However, in practice, we can only focus on the major component of the electromagnetic field, which is $E_y$ in the metallic surface wave structure studied below. Thirdly, in deducing Eq. (5), we neglect the obliquity factor from source point to image point, which works well in the situation of paraxial approximation.

## 4. Near field: single point imaging and focusing

In this section, we use the theory proposed in Sec. III to demonstrate how to get a point image in the near field zone using the theory developed in the above. It is worthwhile to point out that this point imaging can also be treated as a focusing effect [6] in 3D space. We begin with Eq. (6) and choose

$$\alpha_m(x, y) \equiv \alpha \tag{7}$$

$$\psi_0 = -k\sqrt{(p-x)^2+(q-y)^2+l^2} + \varphi' \tag{8}$$

#149847 - $15.00 USD Received 24 Jun 2011; revised 2 Sep 2011; accepted 23 Oct 2011; published 10 Nov 2011

The constant in Eq. (7) stands for carving all grooves with a fixed width and depth. $\psi_0$ in Eq. (8) can be regarded as the phase of a converging wave whose virtual focal point is $F'(p, q, -l)$, as illustrated in Fig. 2(a). $\varphi'$ is introduced to express our formula in a uniform way, as we will see in the following. Then the exponential factor in Eq. (6) equals zero and they lead to

$$U_{img}(p,q,l) \propto \alpha e^{i\varphi'} \sum_m \int_{G_m} \frac{A_r}{\sqrt{(p-x)^2+(q-y)^2+l^2}} ds \tag{9}$$

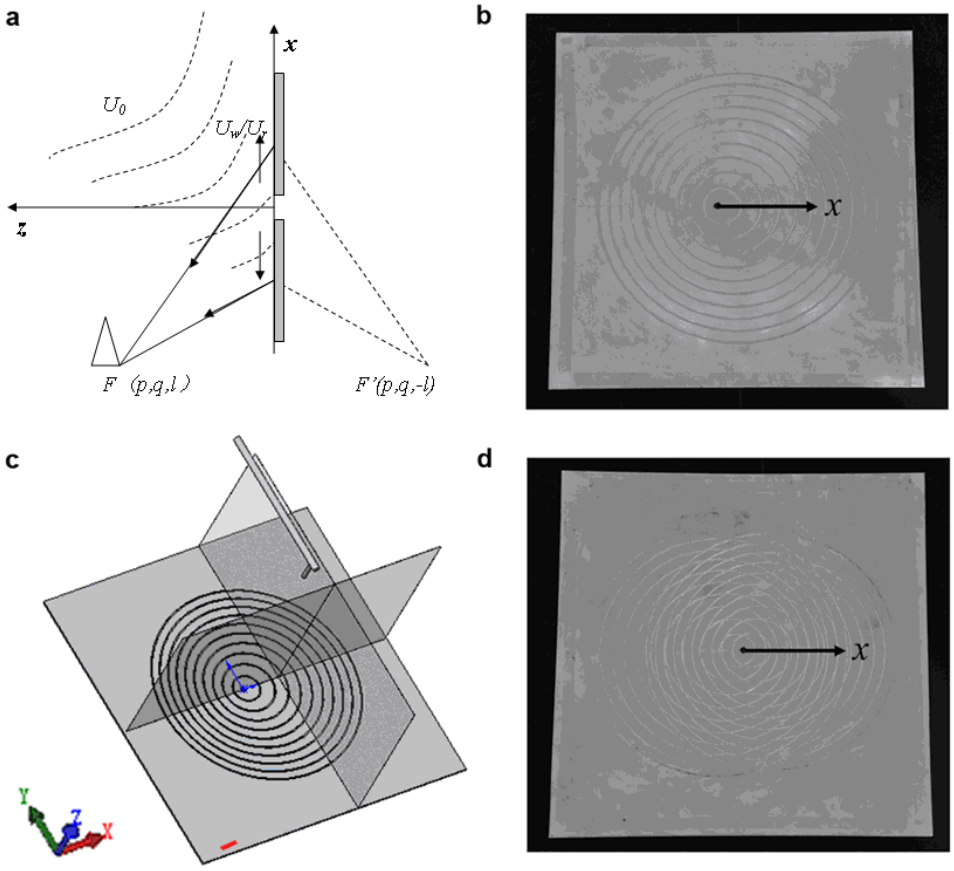


Fig. 2. (a) Schematic of surface wave holography. Metal film is placed in $z = 0$ $xy$ plane. $U_0$ is the incident field, converging to Point $F'$ in the single-point imaging process, whose reconstructed image is focus $F$. An aperture is located at the origin to excite surface wave. (b) Photo of a single-point imaging sample. The focus is designed at (60, 0, 200) mm. $x$ axis is indicated by an arrow and it is normal to the source polarization direction. (c) Schematic of experimental set-up. Source is beneath the aperture. A probe is fixed at a cantilever that can scan in 3 dimensions. Two semi-transparent planes indicate the scanned $x = 60$ mm plane and $y = 0$ mm plane. The red line segment indicates the scale of wavelength. (c) Photo of a two-point imaging sample with two focal spots expected at (–80, 0, 140) mm and (80, 0, 200) mm.

In Eq. (9), all the scatterers in $G_m$ contribute to the wave intensity at ($p$, $q$, $l$) constructively, which makes point ($p$, $q$, $l$) a hot spot. So if we write the metal plate with a wave converging to point ($p$, $q$, $-l$), the reconstituted image is an outgoing wave converging to the focus point located at ($p$, $q$, $l$). Notice that $p$, $q$ and $l$ can take any value here.

Now we can determine the equation of the geometrical morphology of the grooves. Substitute Eq. (8) back into Eq. (2) and we have

#149847 - $15.00 USD Received 24 Jun 2011; revised 2 Sep 2011; accepted 23 Oct 2011; published 10 Nov 2011

$$\sqrt{(p-x)^2+(q-y)^2+l^2}+n_{eff}r=-\frac{\varphi'}{k}+m\lambda \tag{10}$$

In order to satisfy Eq. (10) even when $x = 0$ and $y = 0$, we set $-\varphi'/k=\sqrt{p^2+q^2+l^2}$ , and rewrite Eq. (10) as

$$n_{eff}\sqrt{x^2+y^2}+\sqrt{(x-p)^2+(y-q)^2+l^2}=\sqrt{p^2+q^2+l^2}+m\lambda \tag{11}$$

where $m = 0,1,2\ldots$ This is the equation of the curves of the grooves, which has a clear physical meaning. The first and second term on the left side represent the optical path of the surface wave from the origin (located at the aperture center) to the scattering center and the scattered wave from the scattering point to the investigated point separately, and the first term on the right side is the optical path of wave that directly transmits from the origin to the investigated point. It means that every path from the origin, passing a scattering center, then to point ($p$, $q$, $l$) has the same phase or endures a phase shift by $m\lambda$. All the scattering centers contribute constructively to the wave intensity at ($p$, $q$, $l$). As a result, ($p$, $q$, $l$) is a focus.

According to Eq. (11) we can fabricate our sample of electromagnetic wave focusing. However, some simplifications can be introduced before moving forward. Firstly, no matter where point ($p$, $q$, $l$) is, we can rotate the set of coordinates with respect to $z$ axis to set $q = 0$. Secondly, $n_{eff}\approx 1$ can be used for surface wave in the microwave regime [15, 16, 20]. In this case, we can derive a simple elliptical equation from Eq. (11):

$$\frac{(x-x_0)^2}{a^2}+\frac{y^2}{b^2}=1 \tag{12}$$

where $x_0=\frac{D^2p}{2(L^2-p^2)}$, $a^2=\frac{L^2D^4}{4(L^2-p^2)^2}$, $b^2=\frac{D^4}{4(L^2-p^2)}$, with $L=\sqrt{p^2+l^2}+m\lambda$, and $D^2=L^2-p^2-l^2$. It is the equation of an off-centric ellipse.

Figure 2(b) is the photo of our sample that works in the microwave regime. The wavelength investigated here is 20 mm. Our single-point imaging sample is made with a 3 mm thick aluminum plate. An aperture of 4 mm in radius located at the origin is used to excite the surface wave. The designed focus is situated at $F(p, q, l) = (3\lambda, 0, 10\lambda) = (60, 0, 200)$ mm. A series of off-centric elliptical grooves are carved on a 400 × 400 mm$^2$ plate, whose tracks satisfy Eq. (12) with $m$ varying from 1 to 10. The depth of grooves is 1.5 mm and the width 2.0 mm, which are both much smaller than the 20 mm wavelength. Figure 2(c) is a sketch of our experimental system. A microwave antenna with a 9.5 × 19.0 mm$^2$ window acts as a source and is set 30 mm beneath the aperture. The polarization of the source is normal to $x$ axis [as illustrated in Fig. 2(b)], so are those in the following experiments [Fig. 2(d)]. The total power coming out from the window is 1 mW. A probe is attached to a cantilever to carry out $xy$ scanning at $z = 200$ mm, $zx$ scanning at $y = 0$ mm and $zy$ scanning at $x = 60$ mm. The scanning step is 4 mm.

The parameters of the simulated structure are the same as mentioned above. A plane wave source is placed at 4 mm below the aperture with its polarization normal to $x$ axis, the same as in all the following simulations. A perfect electrical conductor (PEC) is used to model the metal plate. Notice that PEC is a reasonable approximation of metal in the microwave regime. The numerical and experimental results are graphed in Fig. 3. Data in the $z = 200$ mm $xy$ plane, the $y = 0$ mm $zx$ plane and the $x = 60$ mm $zy$ plane are shown. Clear focal points can be recognized in both simulation and experiment. The simulation focal spot, which can be picked out easily, is $F = (60.0, 0.0, 201.9)$mm, slightly different from the expected value. However for experiment, due to the unavoidable noise it is difficult to decide where the precise center of focus is. Our experiment shows that in the $z = 200$ mm $xy$ plane, a maximum is located at (60, 0, 200) mm with a value of 4.36 × 10$^{-7}$ mW, in the $x = 6$ mm $zy$ plane, a maximum of

#149847 - $15.00 USD Received 24 Jun 2011; revised 2 Sep 2011; accepted 23 Oct 2011; published 10 Nov 2011

$4.60 \times 10^{-7}$ mW is located at (60, 0, 206) mm, and in the $y$ = 0 mm $zx$ plane, the (60, 0, 198) mm position has a maximum power of $4.14 \times 10^{-7}$ mW. Both the numerical and experimental results show excellent agreements with design.

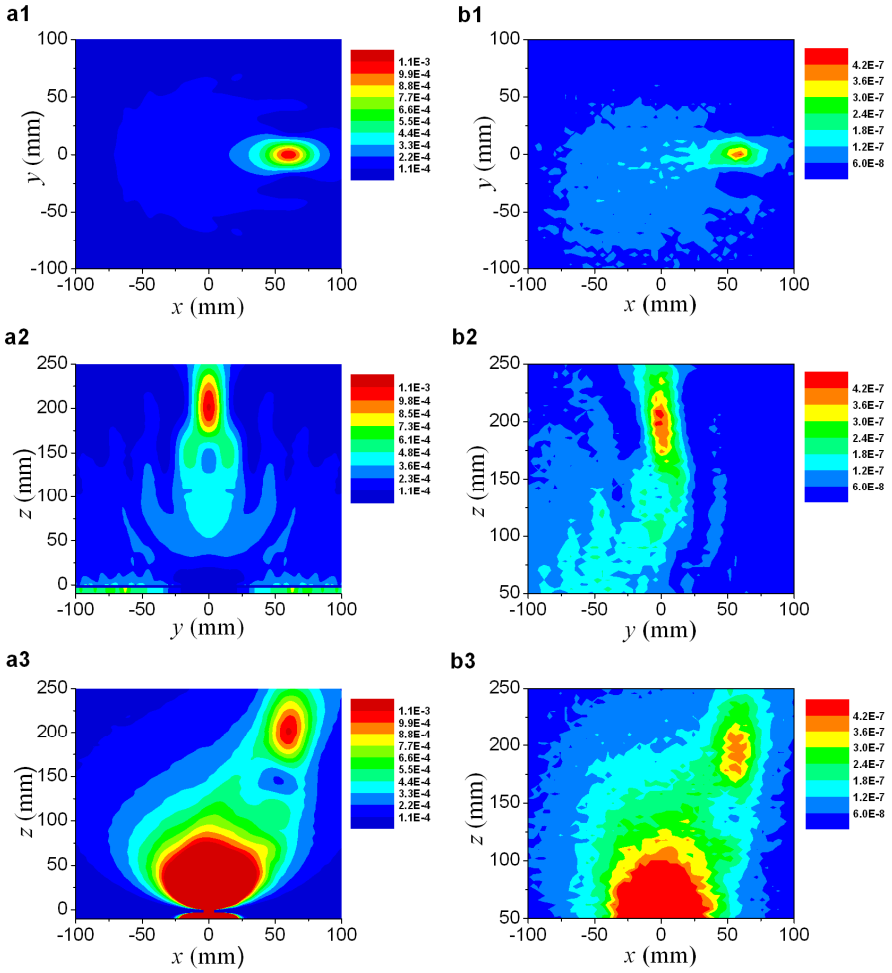


Fig. 3. Field distribution in the upper space of the single-point imaging sample. (a1)~(a3), simulation and (b1)~(b3), experiment. (a1) and (b1) are data of $z$ = 200 mm $xy$ plane, (a2) and (b2) data of $x$ = 60 mm $zy$ plane, (a3) and (b3) data of $y$ = 0 mm $zx$ plane. The scale of z in (a2) and (a3) is (−10, 250) mm, different with (50, 250) mm in (b2) and (b3), in order to give more information. The simulation results are normalized relative to the amplitude of incident plane wave while the unit of experimental results is mW.

Choosing the data in the $z$ = 200 mm plane in Fig. 3(a1) and Fig. 3(b1), the full width at half maximum (FWHM) of the focuses can be determined, which are 20.0 mm for simulation and 20 mm for experiment respectively. It indicates that the structure here can focus electromagnetic wave to the scale of one wavelength, which is the limitation of our imaging capability. In order to give an insightful view, patterns are plotted in Fig. 3(a2) and Fig. 3(a3) with different $z$ scales relative to Fig. 3(b2) and Fig. 3(b3), and they indeed manifest many insightful details. Firstly, in Fig. 3(a2), a scattering pattern is obvious. There are several hot spots immediately above the metal panel, which indicates a strong coupling between the surface wave and grooves, and then the scattered wave front gathers gradually to the focus. Secondly, it can be seen in Fig. 3(a3) the sharply diffracted near field pattern of the aperture. If the source beneath the aperture changes, e.g., the incident direction, the near field pattern

#149847 - $15.00 USD Received 24 Jun 2011; revised 2 Sep 2011; accepted 23 Oct 2011; published 10 Nov 2011

will vary too. However it has very little effect on the focus, which indicates that the imaging effect depends on the incident field weakly.

It can be seen from Fig. 3(b2) that in the region of $y$<0, the noise of the experimental data is more than that in $y$>0. We attribute this phenomenon to the cantilever disturbance during scanning. As shown in Fig. 2(c), the scanning is carried out from $y$>0 to $y$<0. Once the probe is in the $y$<0 region, the reflected and scattered wave from the cantilever will add to the noise. The ratio of the maximum intensity of the imaged focus to the background signal intensity, which is defined as signal-to-noise ratio (SNR) in this paper, is estimated to be about 8:1 in simulation and 4:1 in experiment.

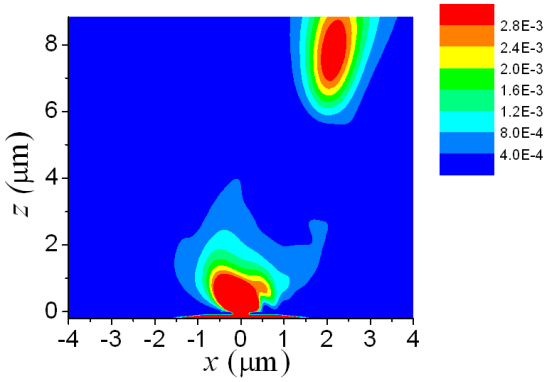


Fig. 4. Simulation of single-point imaging at the wavelength 633 nm. The texture structure is milled on a 150-nm-thick Ag film with the designed focus point located at (1899, 0, 6330) nm. The intensity value is normalized relative to the incident field.

The experiment is carried out in the microwave regime, however our FDTD simulation result of a 150-nm-thick silver sample, using 633 nm visible light, shares the same characteristics as the result shown above. By setting the focus at ($3\lambda$, 0, $10\lambda$) = (1899, 0, 6330) nm, using an aperture of 100nm radius and grooves of 60 nm width and 30 nm depth, and milling the sample according to Eq. (12), we get an image focus at (2140, 0, 7802) nm, which is shown in Fig. 4. The deviation is due to the fact that $n_{eff} \approx 1$ is a rough assumption for textured Ag film in the visible light [15, 27]. Figure 4 indicates that the proposed structure applies from microwave to visible light. By now we can achieve a single-point imaging based on the surface wave holography theory, *viz.*, an arbitrarily focusing effect in 3D space, by writing elliptical grooves on a metal plate in microwave and visible frequencies.

## 5. Far field: image of a plane wave and beam collimation

In this section, we consider the image of a plane wave in the far field zone. Suppose $l$ is much larger than the scale of the textured metal plate, and we set $l\to\infty$, and $p = A\cdot l$, $q = B\cdot l$, where $A$ and $B$ are variables, so that

$$\sqrt{(p-x)^2+(q-y)^2+l^2} \approx \sqrt{1+A^2+B^2}\,l - \frac{Ax}{\sqrt{1+A^2+B^2}} - \frac{By}{\sqrt{1+A^2+B^2}} \qquad (13)$$

Expose the metal with a plane wave with $\boldsymbol{k} = k_0(\sin\theta,\ 0,\ -\cos\theta)$ (the set of coordinates is rotated to set $k_y = 0$) and we have $\psi_0 = k_0 x\bullet\sin\theta$, where $\theta$ is the angle with respect to the $z$ axis. The negative sign in front of $\cos\theta$ stands for the light coming from $z$>0 to $z$<0. Inserting $\psi_0$ and Eq. (13) into Eq. (6), we could write down the outgoing wave

$$U_{img}(p,q,l) \propto \alpha e^{ik\sqrt{1+A^2+B^2}\cdot l} \sum_m \int_{G_m} \frac{A_r}{\sqrt{1+A^2+B^2}\cdot l} e^{ik\left(-\frac{A}{\sqrt{1+A^2+B^2}}+\sin\theta\right)x - ik\frac{B}{\sqrt{1+A^2+B^2}}y} ds \qquad (14)$$

#149847 - $15.00 USD Received 24 Jun 2011; revised 2 Sep 2011; accepted 23 Oct 2011; published 10 Nov 2011

If $B = 0$ and $A/(1 + A^2)^{1/2} = \sin\theta$, the exponential factor equals zero and thus a maximum exists in the far field zone. That is to say when exposing the metal plate with a plane wave whose incident angle is $\theta$, we could see a maximum at ($l\sin\theta$, 0, $l$) in the far field region, which is equivalent to a beam whose outgoing angle is $\theta$.

In this situation, inserting $\psi_0 = k_0 x \bullet \sin\theta = k_0 x \bullet A/(1 + A^2)^{1/2}$ into Eq. (2) gives the geometrical morphology equation of grooves:

$$\frac{Ax}{\sqrt{1+A^2}} - n_{eff}\sqrt{x^2 + y^2} = m\lambda \tag{15}$$

It is worth emphasizing that here $m$ = 0,-1,-2… In 2D condition, Eq. (15) becomes the well known phase matching criterion of SPP grating coupling, $n_{eff}k_0 = k_0 \sin\theta \pm m\Lambda$ , where $\Lambda$ is the grating period [15, 27].

Once again $n_{eff} \approx 1$ is used, and Eq. (15) becomes

$$\frac{(x + m\lambda A\sqrt{1+A^2})^2}{m^2\lambda^2(A^2+1)^2} + \frac{y^2}{m^2\lambda^2(A^2+1)} = 1 \tag{16}$$

It is another elliptical equation. This equation can also be obtained by simply setting $q = 0$, $l \to \infty$, $p/l = A$ in Eq. (14), which corresponds to focusing in an infinite distance.

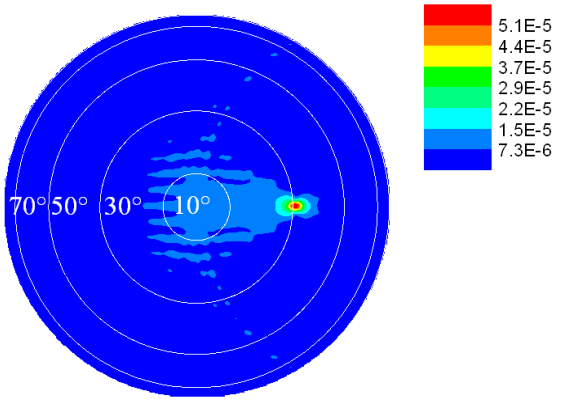


Fig. 5. The simulated plot of far field distribution of plane wave imaging. White circles and numbers indicate the angle $\theta$ with respect to the $z$ axis. A hot spot can be seen at $\theta$ = 31°. The intensity value here is normalized relative to the incident field.

By carving grooves on a metal plate following Eq. (16), we calculate the far field distribution of a far field imaging sample, with the result shown in Fig. 5. $A$ = 0.6 (corresponding to $\theta$ = 31°) is chosen in Eq. (16), and grooves with 2 mm width and 1.5 mm depth are carved on a 3 mm aluminum metal plate with $m$ varying from −1 to −10. The radius of the aperture located at the origin is 4 mm. We can see that at the designated angle $\theta$ = 31° a maximum of microwave intensity does exist.

## 6. Two-point imaging

As narrow and shallow grooves do not change the scattering pattern of the others, one can add two sets of grooves of independent objects on the same metal film. When shining the metal film, the respective two images will come out at the same time. We indeed observed this phenomenon in experiment. According to Eq. (12), we carved two sets of grooves on a 400 × 400 mm$^2$ aluminum plate. The designed focal points are $F_1$ = (−80, 0, 140) mm and $F_2$ = (80, 0, 200) mm. A photo of a two-point imaging sample is shown in Fig. 1(d). The aluminum

#149847 - $15.00 USD Received 24 Jun 2011; revised 2 Sep 2011; accepted 23 Oct 2011; published 10 Nov 2011

metal panel is 3 mm thick, the radius of the aperture is 4 mm, and the width and depth of grooves are 2 mm and 1.5 mm respectively.

Figure 6 shows our simulation and experimental results. Comparing with the single-point sample in Fig. 3(a), the intensity levels of the focal spots in the simulation shown in Fig. 6(a) only diminish a little, instead of half the value relative to the single-point focusing situation. This indicates an incomplete coupling of surface wave into the radiant wave in the single-point sample. In experiment, an antenna with a 9.5 × 19.0 mm window is placed 30 mm beneath the aperture. A scan of $y$ = 0 mm $zx$ plane is shown in Fig. 6(b). Maxima of microwave intensity are observed at points (76, 0, 146) mm and (80, 0, 198) mm. The values of power are $5.47 \times 10^{-7}$ mW and $6.92 \times 10^{-7}$ mW, respectively. They are a little higher when comparing with the result of the single-point experiment. That is because microwave coming out of the antenna window will inevitably diffracts, and a slight misalignment of the position of source relative to the aperture can affect the transmission remarkably. The SNRs in simulation and experiment are roughly 5:1 and 2:1 respectively, which are both lower than those of the single focusing point sample. Theoretically, adding more sets of grooves on the same sample is possible, but that will further reduce the SNR and finally the images would get immersed in the background signals.

We emphasize that the two-point imaging here means two independent point sources in the step of writing the metal plate, i.e., first expose the metal plate with Source A and then expose with Source B. It is different from writing an object with two points separated in space. In other words, many objects can be written on a same plate. One feasible application of this feature is multi-path coupling and output of nanolaser, and in a reverse process, it can be used to excite a spot effectively by using several beams.

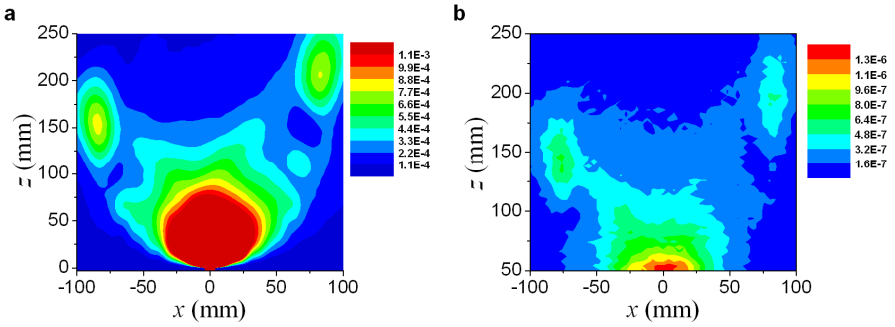


Fig. 6. Field distribution on the $y$ = 0 mm $zx$ plane of the two-point imaging sample. (a) Simulation. (b) Experiment. Different $z$ scales are used here too. As before the simulation results are normalized value and the unit of experimental results is mW.

From the simulated and experimental results shown above, the design method based on Eq. (6) really works well despite the fact that several approximations have been made to derive Eq. (6). It is worth noting that in all the simulations and experiment above, we use well-defined polarized sources, $y$ polarized, which is the main polarization component in our systems, so considering $E_y$ and neglecting $E_x$ and $E_z$ of the system is acceptable. In fact, our FDTD calculations show that the intensity distribution of $E_x^2 + E_y^2 + E_z^2$ and $E_y^2$ based on structure in Fig. 3 is of little difference. As a result, Eq. (6) works well although it only considers a single polarization component. To be more accurate, a more complete theory of Eq. (6) needs to be developed, however, this makes a simple design of metallic surface wave structure almost impossible.

## 7. Summary

Our simulation results show that when a surface electromagnetic wave passes a groove whose size is much smaller than the wavelength, both the intensity and phase of the surface wave change little. On the basis of this property, we propose a method using surface wave

#149847 - $15.00 USD Received 24 Jun 2011; revised 2 Sep 2011; accepted 23 Oct 2011; published 10 Nov 2011

holography theory to design textured metallic film to realize a given functionality, which is applicable from microwave to visible light. In the framework of this method, a focusing effect in 3D space can be regarded as an imaging process of a virtual point source, and a beam collimation of light at any solid angle as an imaging process of a plane wave source. In addition, independent objects can be exposed on the same metal film, and all images will exist at the same time when shined.

The good agreement between our numerical and experimental results has confirmed the power of this analytical approach. The theory not only provides a new angle of view to understand and exploit subwavelength structures on a metallic surface but also opens a new path for designing metallic surface morphologies to realize complicated functionalities of electromagnetic wave transport in 3D space. As the method originates from a fact that negligible additional phase shift exists when surface wave passes a small groove, we expect that this characteristic is shared by many other subwavelength devices and it can be used to design the optical devices of more complicated functions. More interestingly, the property of independent-object writing, which was hardly studied before, may find applications in fields such as imaging, high density storage, high sensitive detecting and multi-beam excitation. The great application potential of this method is worthy of intensive and extensive exploration.

**Acknowledgments**

This work was supported by the National Natural Science Foundation of China under Grant Nos. 60736041 and 10874238, and the National Key Basic Research Special Foundation of China under Grant No. 2007CB613205 and 2011CB922002.

#149847 - $15.00 USD Received 24 Jun 2011; revised 2 Sep 2011; accepted 23 Oct 2011; published 10 Nov 2011